Available online at www.sciencedirect.com
ScienceDirect
Journal of Solid State Chemistry 179 (2006) 3814–3823
JOURNAL OF SOLID STATE CHEMISTRY
www.elsevier.com/locate/jssc

V_2O_5 xerogel–poly(ethylene oxide) hybrid material: Synthesis, characterization, and electrochemical properties

Elidia M. Guerra[a], Kátia J. Ciuffi[b], Herenilton P. Oliveira[a,*]

[a]*Departamento de Química, Faculdade de Filosofia, Ciências e Letras de Ribeirão Preto, Universidade de São Paulo, 14040-901 Ribeirão Preto-SP, Brasil*
[b]*Universidade de Franca, Av. Dr. Armando Salles Oliveira 201, P.O. Box 82, 14404-600 Franca, SP, Brasil*

Received 28 June 2006; received in revised form 16 August 2006; accepted 21 August 2006
Available online 23 August 2006

Abstract

In this work, we report the synthesis, characterization, and electrochemical properties of vanadium pentoxide xerogel–poly(ethylene oxide) (PEO) hybrid materials obtained by varying the average molecular weight of the organic component as well as the components' ratios. The materials were characterized by X-ray diffraction, ultraviolet/visible and infrared spectroscopies, thermogravimetric analysis, scanning electron microscopy, electron paramagnetic resonance, and cyclic voltammetry. Despite the presence of broad and low intensity peaks, the X-ray diffractograms indicate that the lamellar structure of the vanadium pentoxide xerogel is preserved, with increase in the interplanar spacing, giving evidence of a low-crystalline structure. We found that the electrochemical behaviour of the hybrid materials is quite similar to that found for the V_2O_5 xerogel alone, and we verified that PEO leads to stabilization and reproducibility of the Li^+ electrochemical insertion/de-insertion into the V_2O_5 xerogel structure, which makes these materials potential components of lithium ion batteries.

Keywords: Vanadium pentoxide xerogel; Poly(ethylene oxide); Intercalation; Electrochemistry; Hybrid compound

1. Introduction

From a general point of view, the combination of different organic/inorganic components in a single material may lead to unique electrical, optical, and mechanical properties that may not be present in the starting components alone [1–4]. As a consequence, interests in this field have increased with regard to both the fundamental understanding and the potential applications of new organic–inorganic hybrid materials in several areas, such as catalysis, electrochromic devices, and energy storage [1–4]. Concerning the last item, an increasing number of polymer–inorganic hybrid compounds have been investigated as promising materials for battery cathodes [5–7]. In particular, hybrid materials based on the vanadium pentoxide xerogel have attracted much attention as battery cathodes in the last two decades, because they combine a layered structure suitable for the insertion reaction with electrochemical properties and a mixed ionic–electronic conductivity [6–10]. Unfortunately, a decrease in the charge–discharge capacity of the V_2O_5 xerogel is normally observed after some cycles, a fact that could be attributed to solvent exchange, steric hindrance limiting rechargeability, and irreversible changes in the structure [11,12]. Thus, in order to improve lithium ion diffusion and electrochemical stability, intrinsic conductive polymers such as polyaniline and polypyrrole have been extensively used to prepared transition metal oxide-based hybrid materials [6–8]. Another approach to increase lithium ion diffusion has been to intercalate non-intrinsic conducting polymers such as poly(ethylene oxide) (PEO), to enhance the ionic conductivity in lamellar and porous electrolytes [13–15]. For example, Aranda and Ruiz-Hitzky [13] synthesized PEO/montmorillonite nanocomposites, which led to an increase in the distance between the silicate layers and facilitated the mobility of the interlayer ions. They found that these nanocomposites were thermally stable and exhibited ionic conductivity (10^{-5} S/cm) associated with the motion of the intracrystalline cations over a

*Corresponding author. Fax: +55 16 3602 4838.
E-mail address: herepo@ffclrp.usp.br (H.P. Oliveira).

0022-4596/$ - see front matter © 2006 Elsevier Inc. All rights reserved.
doi:10.1016/j.jssc.2006.08.018

broad temperature range [13]. By means of NMR experiments, Reinholdt et al. [15] showed that the differences in conductivity values found for the Li-PEO/montmorillonite and Na-PEO/montmorillonite nanocomposites could be correlated with the difference in hydration between the two cations. Mai et al. [16] reported that modification of the MoO_3 xerogel films by PEO leads to a better electrochemical performance of the matrix. Concerning the PEO/V_2O_5 layered system, previous studies have indicated that it leads to interesting lithium redox intercalation, photochemical, and electrical properties [17–20]. By using NMR spectroscopy, authors of these studies stated that the $Li_y(PEO)_x \cdot V_2O_5 nH_2O$ materials exhibit the mobility of lithium ions in the intracrystalline structure, leading to good ionic conductivity [17,18]. Moreover, in a further investigation, using Ac impedance and conductivity measurements, Kloster et al. [19] demonstrated that the V_2O_5/[$(CH_2O)(CH_2CH_2O)_{(8.7)}$](n)-$LiCF_3SO_3$ nanocomposite exhibits both electronic and ionic conductivities and the total conductivity is highly anisotropic. Exploiting the layered structure of the V_2O_5 xerogel, Chen et al. [21] showed that its modification by PEO improves the reversibility of Li^+ ion insertion/extraction, probably because of the strong interaction between the host and the guest species, which shields the electrostatic interaction between the V_2O_5 interlayer and the Li^+ ions, thus leading to better cyclability [21]. However, a detailed investigation of the electrochemical properties of V_2O_5 xerogel–PEO hybrid materials seems to be interesting, because it would enable one to explore their potentiality as constituent elements in cathodes for lithium ion battery and it would help describe the mechanism through which the introduction of PEO into the host structure improves cyclability. In this context, our interest is to investigate the reversibility of Li^+ ion insertion/de-insertion into V_2O_5 xerogel films resulting from the presence of PEO in the interlayer domain of the host structure. Moreover, we aimed at studying how different amounts of PEO and its average molecular weight influences the chemical composition, crystallinity, and electrochemical properties of the hybrid materials when this polymer is inserted into the V_2O_5 interlayer.

2. Experimental section

2.1. Reagents

All chemicals used in this work were reagent grade and were used without any previous treatment. PEO, with average molecular weights (MW) of 100,000, 300,000, and 600,000 g/mol, was purchased from Acros. Acetonitrile was chromatographic grade (Fluka), the vanadium pentoxide xerogel was prepared from sodium metavanadate (Fluka), and the ion-exchange resin was Dowex-50X in its acid form. Water was purified using a Millipore Milli-Q System.

2.2. Preparation of the V_2O_5 gel

The vanadium pentoxide gel, $V_2O_5 \cdot nH_2O$, was prepared from sodium metavanadate ($NaVO_3$, 99%, Fluka) by the ion exchange method (ion-exchange resin Dowex-50X), as described in the literature [22,23]. A decavanadic acid was obtained by percolating 0.10 mol/dm^3 of a $NaVO_3$ aqueous solution through a cationic ion-exchange resin. Upon standing at room temperature (24 °C) for 2 weeks, the fresh HVO_3 solution was polymerized leading to a viscous red V_2O_5 gel. Syntheses of all the hybrid compounds were performed on 2-month-aged gel. Thermogravimetric analysis was carried out to evaluate the water content in the corresponding vanadium pentoxide xerogel: $V_2O_5 \cdot 2.0H_2O$.

2.3. Preparation of the V_2O_5/PEO hybrid material

In a typical preparation, 5.00 mL of an aqueous solution of PEO (2.5×10^{-7}, 160×10^{-7}, 360×10^{-7} mol/dm^3) were added to V_2O_5 gel (10.0 mL) under constant stirring for 48 h. The resulting brown suspension was cast into a film form by evaporation of water at room temperature on a glass or another flat substrate (e.g., glassy carbon electrode). Afterwards, the resulting film was rinsed with deionized water and dried again at room temperature. The color of the film was light brown with metallic luster. The samples were named as follows:

PEO MW (g/mol)	PEO solution 2.5×10^{-7} mol/dm^3	PEO solution 160×10^{-7} mol/dm^3	PEO solution 360×10^{-7} mol/dm^3
100,000	PEOV125	PEOV1160	PEOV1360
300,000	PEOV325	PEOV3160	PEOV3360
600,000	PEOV625	PEOV6160	PEOV6360

The composition of the hybrid materials, shown in Table 1, was determined by elemental and thermogravimetric analyses.

2.4. Equipment and procedure

The X-ray diffraction (XRD) data were recorded on a SIEMENS D5005 diffractometer using a graphite monochromator and CuK_α emission lines (1.541 Å, 40 kV, 40 mA). To this end, samples in the film form and deposited onto a glass plate were employed, and the data were collected at room temperature over the range $2^\circ \leqslant 2\theta \leqslant 50^\circ$, with a step of 0.020°. Fourier-transform infrared spectra (FTIR) were recorded from 4000 to 400 cm^{-1} on a Bomem MB 100 spectrometer, and the samples were dispersed in KBr and pressed into pellets. The transmission electronic spectra (ultraviolet/visible spectra, UV/Vis) were recorded on a Varian Cary 50 spectrophotometer. Electron paramagnetic resonance (EPR) spectra were obtained at room temperature using a computer interfaced Varian E-4 spectrometer operating

Table 1
Composition of the V_2O_5/PEO hybrid materials obtained from elemental and thermogravimetric analyses

Sample	Composition	Sample	Composition	Sample	Composition
PEOV125	$(V_2O_5)(PEO)_{0.05}(H_2O)_{1.6}$	PEOV325	$(V_2O_5)(PEO)_{0.06}(H_2O)_{1.5}$	PEOV625	$(V_2O_5)(PEO)_{0.05}(H_2O)_{1.5}$
PEOV1160	$(V_2O_5)(PEO)_{1.9}(H_2O)_{0.6}$	PEOV3160	$(V_2O_5)(PEO)_{3.2}(H_2O)_{0.4}$	PEOV6160	$(V_2O_5)(PEO)_{2.7}(H_2O)_{1.1}$
PEOV1360	$(V_2O_5)(PEO)_{6.1}(H_2O)_{0.8}$	PEOV3360	$(V_2O_5)(PEO)_{11}(H_2O)_{1.8}$	PEOV6360	$(V_2O_5)(PEO)_{7.1}(H_2O)_{1.2}$

at 9.5 GHz (X band). For these measurements, the samples were positioned so that the magnetic field was perpendicular to the orientation of the sample surface. Scanning electronic microscopy (SEM) studies were carried out on a ZEISS-DSM 940 microscope operating at 20 kV. Cyclic voltammograms were measured using an AUTOLAB (EcoChemie) model PGSTAT30 (GPES/FRA) potentiostat/galvanostat interfaced with a computer. The conventional electrode arrangement was used, which consisted of glassy carbon as supporting electrode, a platinum wire auxiliary electrode, and saturated calomel electrode (SCE) as reference. The intercalation compounds were deposited on the electrode surface by evaporating approximately 5 μl of the suspension at room temperature (24 °C). The supporting electrolyte studied in acetonitrile medium was 1.0 mol/dm^3 $LiClO_4$. In addition, all the experiments were carried out in deoxigenated solutions by bubbling N_2, and at room temperature. Elemental analysis (carbon and hydrogen) was performed using an Elemental Analyzer CE Instruments, model EA-1110, and data were obtained by means of the Dynamic Flash Combustion method. The thermogravimetric data were registered on a Thermal Analyst equipment model 2100-TA in air atmosphere, at a heating rate of 10 K/min.

3. Results and discussion

Fig. 1 shows the thermogravimetric curves of the V_2O_5/PEO hybrid compounds. Weight losses and the respective temperature ranges are reported in Table 2. For the hybrid compounds, the thermogravimetric curves (Figs. 1a–c) show three weight loss events, with maximum loss rate taking place between 423 and 693 K, followed by a slight mass increase up to 873 K for the materials prepared with 2.5×10^{-7} or 160×10^{-7} mol/dm^3 PEO aqueous solution, and a continuous mass decrease was observed up to 873 K for the materials prepared with 360×10^{-7} mol/dm^3 PEO aqueous solution. The first weight loss in the 303–423 K range can be attributed to loss of adsorbed water molecules. The second step of the thermogravimetric plot in the 423–693 K range corresponds to a major weight loss event. This event may involve not only the loss of weakly bound water molecules and coordinated/interlayer water molecules present in the hybrid materials, but also decomposition of the organic polymer [15,19,24]. Moreover, the release of strongly bound water molecules from vanadium pentoxide can also be associated with this temperature range, consequently leading to the formation of crystalline vanadium pentoxide at temperatures above 623 K [25,26]. Finally, the third step (>693 K) is attributed to gradual loss of residual hydroxyls and to PEO decomposition, and it can also be related to the transformation of the vanadium pentoxide xerogel into crystalline vanadium pentoxide [15,19,24]. Concerning the mass increase up to 873 K for the materials prepared with 2.5×10^{-7} and 160×10^{-7} mol/dm^3 PEO aqueous solution, this event might be due to the formation of V^{IV} sites together with anion vacancies (O^{2-} ions and hydroxyl groups on oxygen sites) during the heating under air atmosphere and in the presence of water molecules. Therefore, the V^{IV} species are oxidized to V^{V} upon continuous heating, leading to the formation of crystalline vanadium pentoxide.

Figs. 2a–f show the X-ray diffraction patterns for the V_2O_5/PEO hybrid compounds and for the vanadium pentoxide xerogel matrix (Fig. 2g). From a general point of view, diffraction patterns of the hybrid materials show the presence of broad peaks, suggesting that these materials have low crystallinity, with a bi-dimensional structure similar to that of the V_2O_5 xerogel matrix. The most intense diffraction peak (00 *l*) is characteristic of the one-dimensional stacking of the vanadium pentoxide xerogel ribbons perpendicular to the substrate [23,27,28]. Therefore, the presence of the typical diffraction peaks (00 *l*) in the XRD patterns of the hybrid compounds indicate a layered framework due to showing that the lamellar structure of the V_2O_5 xerogel is maintained (shown in Fig. 2g), which is consistent with a topotactic process. In addition, the shifts of the 0 0 1 reflection to lower 2θ values indicate there is an increase in the interlayer spacing, which is consistent with the presence of the polymeric species in the matrix (*d*-spacing of 11.7 Å), as can be seen in Table 3. There is an increase in the interlayer distance when the amount of the polymeric species is raised in the case of the V_2O_5/PEO hybrid materials containing MW_{PEO} = 100,000 g/mol. As for the V_2O_5/PEO hybrid materials with MW_{PEO} = 300,000 g/mol, there also is an increase in the interlayer distance at higher concentration. The interlayer distance value found for PEOV325 is lower than those found for PEOV3160 and PEOV3360, which have approximately the same value. Concerning the V_2O_5/PEO composites with MW_{PEO} = 600,000 g/mol, similar results are obtained if compared with the other composites containing PEO of different molecular weights, and an increase in the interlayer distance occurs when the PEO concentration is raised. Probably, this increase in *d*-spacing is an evidence of

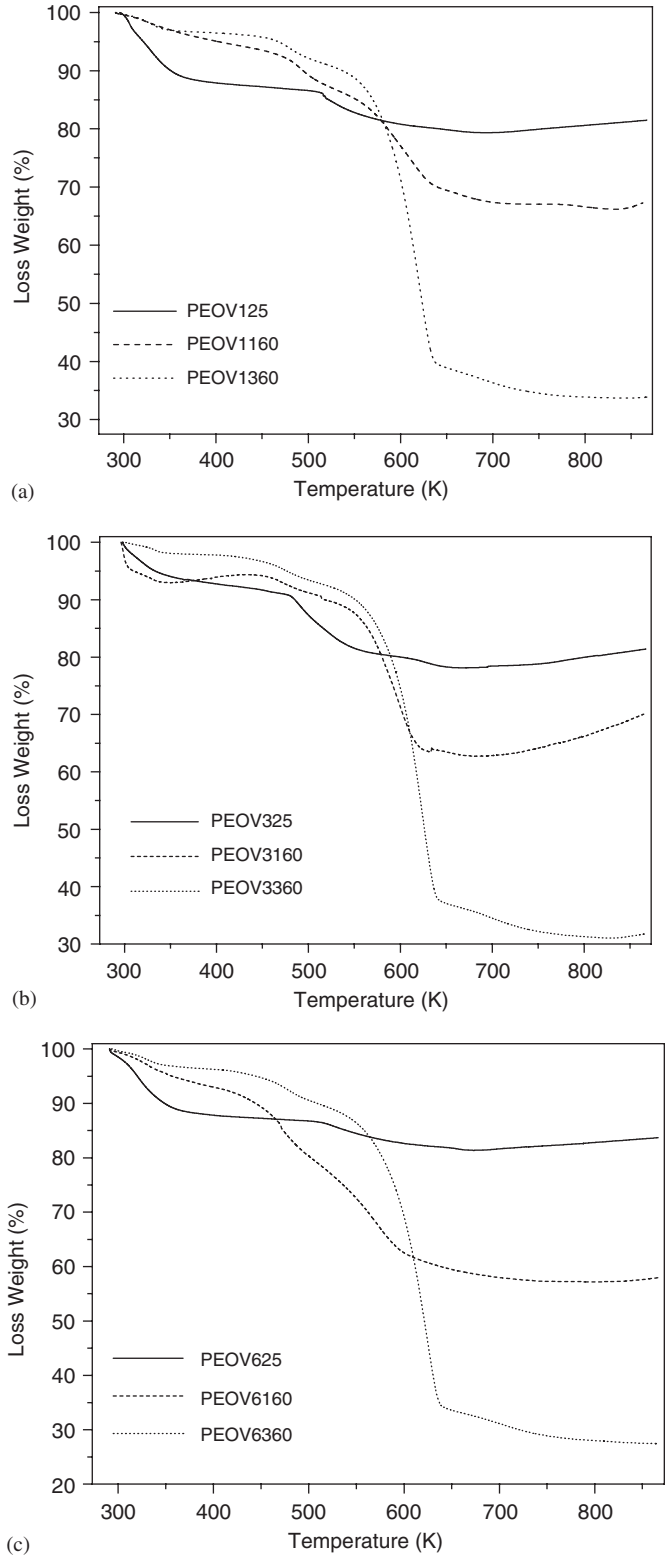

Fig. 1. Thermogravimetric curves of (a) PEOV125, PEOV1160, and PEOV1360; (b) PEOV325, PEOV3160, and PEOV3360; (c) PEOV625, PEOV6160, and PEOV6360.

the replacement of the weakly bound interlamellar water molecules with polymeric species. Although these data provide an indication that the polymers lie in the interlayer region, the presence are of surface-sorbed polymer molecules on the edges of the inorganic matrix cannot be ruled out. Another point is that the widest variation in *d*-spacing for the hybrid materials in relation to the matrix is approximately 8.8 Å, except for the materials with a low PEO amount. This fact may be related to the presence of a single layer of organic polymer inserted into the interlayer domain. Liu et al. have stated that the different interlayer expansion can be associated with the self-assembly of the composite after intercalation [18]. They suggested that a net expansion around 4.0 Å is too small for a helical structure, being this value more consistent with a planar zigzag conformation [18]. However, a net expansion of 8.0 Å or higher may be due to the presence of either two layers of polymer chains with a planar zigzag conformation or one layer of helical PEO. In comparison with the results presented in Table 3, it is possible to assume that the composites may adopt a planar zigzag conformation, except for the PEOV6160 hybrid material, which presents a lamellar spacing of 8.82 Å, typical of a bilayer arrangement of polymeric chains in a planar zigzag conformation. The average crystallite size of the hybrid V_2O_5/PEO compounds was estimated from the width of the main diffraction peak (*001*), by using the Scherrer equation: $L_{hkl} = K\lambda/B\cos\theta$ (L is the crystallite size, λ is the X-ray wavelength, K is the Scherrer's constant and has a value of 0.9, θ is the Bragg angle, and B is the peak width at half-height in radians). Taking the average crystallite size values (Table 3) into account, the hybrid materials have lower crystallinity when compared with the matrix ($L \approx 316$ Å). This observation may be attributed to an increase in the stacking disorder after intercalation, which occurs because of a mechanical stress of the inorganic host in relation to the free matrix. In addition, a linear expansion in the interlayer distances is absent in all the hybrid materials, independent of the PEO average molecular weight. This is a result of the conformational changes undergone by PEO when it is placed between the layers of the matrix layers [18].

The infrared spectra of the vanadium pentoxide xerogel matrix and the PEO (300,000 g/mol) between 4000 and 400 cm^{-1} are shown in Figs. 3a, b. Because the spectra of the hybrid materials are quite similar, they are represented by the spectrum of the PEOV3160 sample (Fig. 3c). The vibrational spectrum of the vanadium pentoxide xerogel (Fig. 3a) has been previously discussed [29–31]. The band at 1010 cm^{-1} has been ascribed to the V–O stretching of the vanadyl group (V = O), and the bands at 762 cm^{-1} and at 536 cm^{-1} are related to ν_{asym}(V–O–V) and ν_{sym}(V–O–V) vibration modes associated with the vanadium-oxide bridges, respectively. In the hybrid compound (Fig. 3c), they are found at 1020, 740 and at 510 cm^{-1}, respectively. The infrared spectrum of PEO (Fig. 3b) is characterized by the presence of two bands related to CH_2 rocking modes in the 800–100 cm^{-1} region (843 and 957 cm^{-1}). In addition, this spectrum also shows a broad band in 1050–1220 cm^{-1} region ascribed to the stretching modes of the C–O–C

Table 2
Percentage weight losses during the increase of temperature

Hybrid compound	Weight loss (%)		
	Temperature range (K) 303–423	Temperature range (K) 423–693	Temperature range (K) 693–873
PEOV125	12	8.9	+1.9
PEOV1160	6.8	25.8	0
PEOV1360	3.5	59.7	3.2
PEOV325	7.8	13.8	+3.0
PEOV3160	5.9	31.6	+7.5
PEOV3360	2.8	62.6	3.1
PEOV625	12.6	6.0	+2.5
PEOV6160	8.1	34	+0.2
PEOV6360	4.1	64.6	4.2
Possible event	Dehydration	Dehydration/decomposition	V_2O_5 crystalline

Observation: + is an indication of gain of weight.

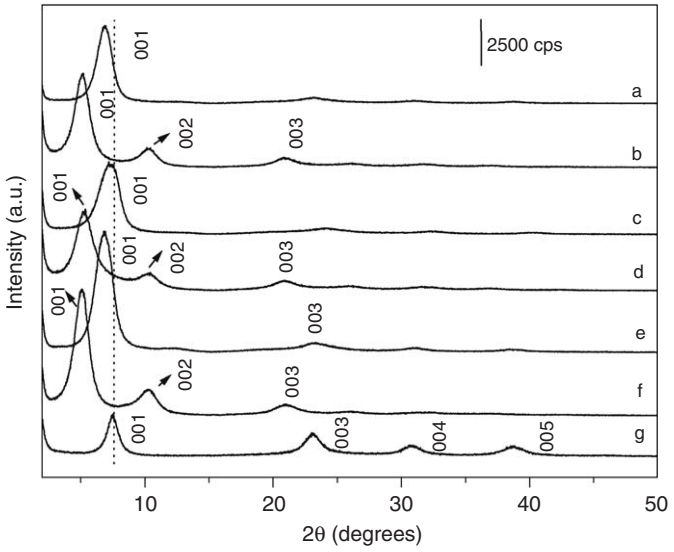

Fig. 2. X-ray diffraction patterns of the samples: (a) PEOV125; (b) PEOV1360; (c) PEOV325; (d) PEO3360; (e) PEOV625; (f) PEO6360; (g) vanadium pentoxide xerogel ($V_2O_5 \cdot 2.0H_2O$).

Table 3
Values of the interlayer distances (d), variation of the interlayer distances and of the composite V_2O_5/PEO in different molecular weights of PEO

Hybrid material	d_{001} (Å)	Δd (Å)	Average crystallite size (Å)
PEOV125	13.0	1.30	243
PEOV1160	17.6	5.90	225
PEOV1360	18.0	6.30	246
PEOV325	12.1	0.40	179
PEOV3160	17.5	5.84	382
PEOV3360	17.8	6.13	236
PEOV625	13.0	1.28	232
PEOV6160	20.5	8.82	353
PEOV6360	17.6	5.88	264

group [33,34]. In the region between 1200 and 1500 cm^{-1}, there are four bands related to CH_2 vibrational modes: the bands at 1241 and 1283 cm^{-1} are attributed to twisting

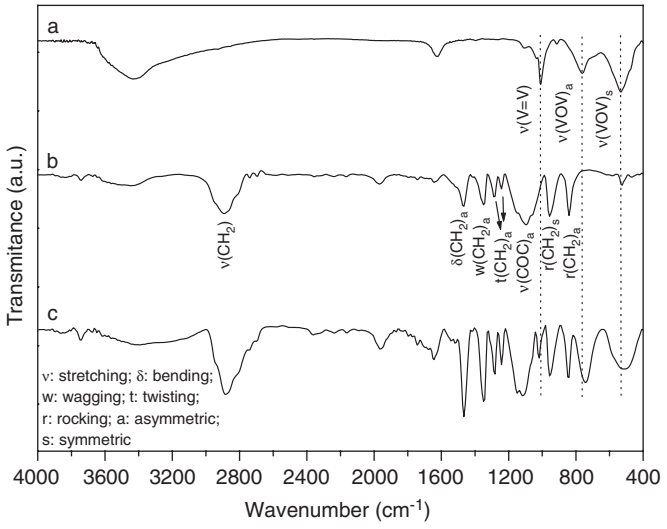

Fig. 3. FT-IR spectra of the samples: (a) vanadium pentoxide xerogel ($V_2O_5 \cdot 2.0H_2O$); (b) PEO (300,000 g/mol); (c) PEOV3160.

vibration, while the one at 1347 and 1467 cm^{-1} are assigned to the wagging and bending modes, respectively [18,24,32–34]. An intense absorption in the 2750 cm^{-1} region due to CH_2 stretching mode is also observed. The FTIR spectra of the compounds intercalated with PEO of different average molecular weight (Fig. 3c) are not significantly different; even though the intercalation compounds were obtained from different starting solutions, which resulted in materials with different contents of the organic material. In relation to organic polymer's structure, the hybrid material' spectrum (Fig. 3c) does not show any significant vibrational mode shift by comparing with the bulk PEO's spectrum (Fig. 3b). In contrast, concerning the V_2O_5 framework, the $\nu(V=O)$ mode is slightly shifted to higher wavenumber (1020 cm^{-1}), whereas the V–O–V vibrational modes shifted to lower wavenumbers: $762 \rightarrow 740\ cm^{-1}$; $536 \rightarrow 510\ cm^{-1}$. Besides, it should be noted that these bands became broader. The shift of the $\nu(V=O)$ mode may be related to the strengthening of the V = O bond. On the contrary, the downshifts of ν(V–O–V)

vibrational modes after the incorporation of the organic polymer implies in a weakening of these bonds. These spectral changes observed here suggest a distortion in coordination geometry at the metal centre, probably arising from steric interactions between the confined polymer and the V_2O_5 framework [18]. However, these results indicate that the structure of the layered vanadium pentoxide is preserved after the reaction, despite the low crystallinity and the polymer content.

The ultraviolet/visible electronic spectra of the vanadium pentoxide xerogel matrix and of the V_2O_5/PEO hybrid compounds (not shown) are quite similar. The electronic spectra display two intense absorption bands in the ultraviolet region: at 268 and 389 nm, attributed to the vanadium (V)-oxide charge-transfer bands [22,35,36]. The absorption bands at 389 nm and 268 nm can be associated with the $b_1(\pi)\rightarrow b_2(xy)$ and $a_2(\pi)\rightarrow b_2(xy)$ transitions involving vanadium ions and the four equatorial oxygen atoms, respectively [36,37]. In addition, low-intensity *d–d* transitions of the vanadyl groups in the 600–800 nm range are absent in the spectra, since the intensities of these transitions depend on the amount of V^{IV} ions. The absence of bands in this spectral range suggests that the vanadium species are mostly present in their oxidized form. However, the presence of a low amount of V^{IV} cannot be ruled out. Thus, the polymeric species do not significantly affect the absorption bands of the matrix, which gives evidence of the weak interaction between the host structure and the organic polymers.

EPR spectra of the vanadium pentoxide xerogel and of PEOV325, PEOV3160 and PEOV3360 hybrid compounds at room temperature are shown in Fig. 4. The spectrum of the matrix (Fig. 4a) is typical of the V^{4+} ion in an axially distorted crystal field; i.e., it is dominated by the axial hyperfine interaction between the unpaired electron spin ($S = 1/2$) and the ^{51}V nuclear spin ($I = 7/2$) and is characteristic of rigid limit VO^{2+} systems (V^{4+}, d^1) [22,38]. Therefore, an eight-component hyperfine structure is expected from the dipole–dipole interaction between the magnetic moment of the ^{51}V nucleus and the electronic moment of the paramagnetic V^{4+} ions. In addition, this hyperfine splitting is sensitive to the chemical environment around the paramagnetic V^{4+} ion. In the case of the spectra of the hybrid materials, shown in Figs. 4 b–d, slight changes in the EPR spectrum are observed. The signal is dominated by the host, with a broadening of the EPR line centred on $g = 1.96$, typical of the vanadium pentoxide xerogel. Probably, the broad signal and the lack of a well-resolved fine structure in the EPR spectrum of the V_2O_5 xerogel can be related with magnetically interacting V^{4+} centres, which consisted of clusters or pairs of vanadium ions close enough to cause dipolar broadening of the EPR signal. In other words, as the content of V^{4+} increases ($V^{4+}/V^{4+}+V^{5+}$ ratio $>2\%$), the hyperfine

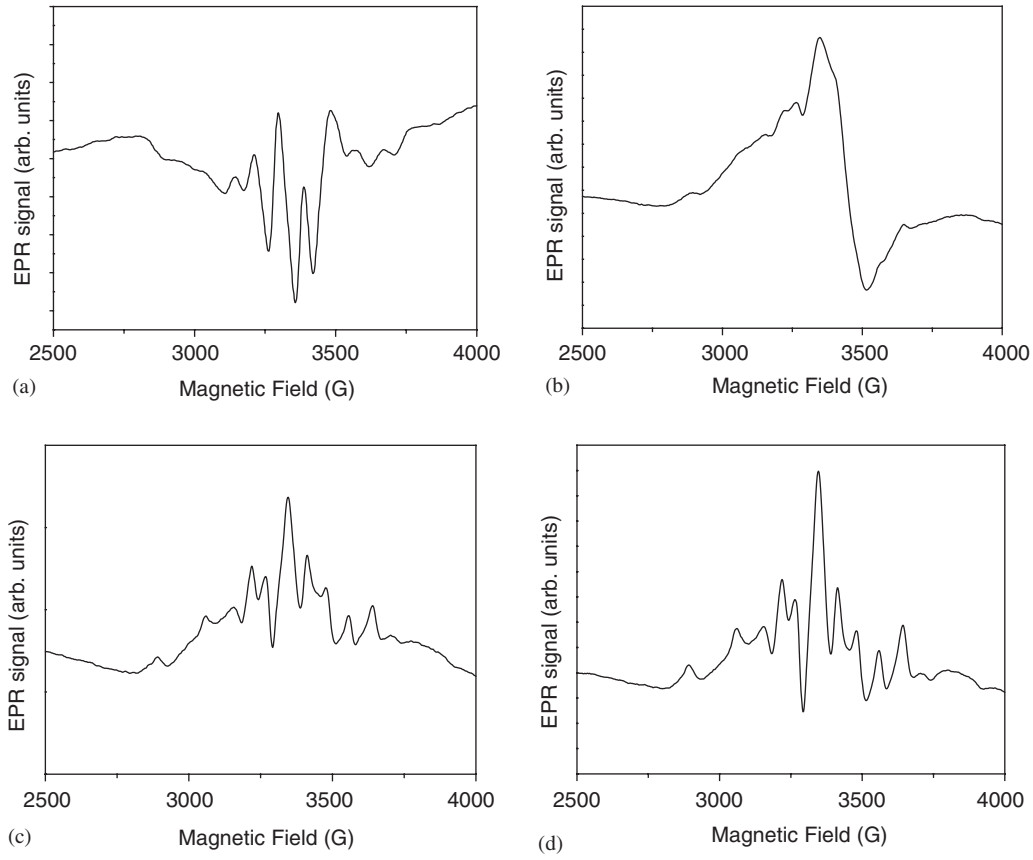

Fig. 4. EPR spectra of (a) vanadium pentoxide xerogel ($V_2O_5 \cdot 2.0H_2O$); (b) PEOV325; (c), PEOV3160; (d) PEOV3360.

EPR interactions tend to disappear [39]. The loss of resolution observed in the EPR spectrum (Figs. 4b–d) may indicate a redistribution of the V^{4+} centres, so that they become close enough to interact with each other. This suggests that these centres are not evenly distributed through the hybrid materials because of the low crystallinity of the materials attributed in the increase of the stacking disorder after intercalation. Furthermore, after the reaction with the polymer molecules, we did not observe any apparent change in the oxidation state of the vanadium ions that could lead to the broadening of the EPR line.

To summarize, the characteristics of these hybrid materials are similar but not identical to those found in other reports [18,21]. Liu et al. [18] state that PEO intercalation does not affect the structural integrity of the V_2O_5 matrix based on FT-IR and X-ray diffraction data. Although, the authors had observed some difference in relative intensities and band shapes between intercalated and bulk PEO, by comparing both FT-IR spectra. In addition, the electronic spectra of the intercalation compounds are nearly identical with that of the V_2O_5 xerogel [18]. Moreover, the authors observed the EPR hyperfine structure in the spectra of PEO/V_2O_5 materials attributed to $(V=O)^{2+}$ impurities in an axially distorted crystal field. In contrast, Chen et al. [21] verified a downshift of the $\upsilon(V=O)$ and that V–O–V modes shifted to higher wavenumbers. They attributed these effects to hydrogen bond, i.e., the hydrogen atoms of the organic polymer are bonded with the oxygen atoms of the V = O species leading to shifts of the V_2O_5 framework's vibrational modes. Concerning our results, they corroborate the Liu's findings, independent the amount and the average molecular weight of the organic polymer into V_2O_5 lamellar structure. Overall, both the PEO and vanadium pentoxide xerogel bands are not significantly shifted, suggesting that a slight distortion occurs when the organic polymer is present into the lamellar structure of the matrix in agreement with the diffraction data discussed above.

Fig. 5 shows scanning electron micrographs of the V_2O_5 xerogel and the V_2O_5/PEO hybrid compounds, which allow us to examine the possible changes in surface morphologies. The micrographs of other hybrid materials are similar when compared with these images in Fig. 5. In the SEM image of the hydrated vanadium pentoxide matrix (Fig. 5a) there is evidence of a network of randomly oriented interconnected chains [10,23]. In contrast, the SEM images of the hybrid materials (Figs. 5b–d) show how the morphology changes, forming a smooth and homogeneous surface. In addition, there are not cracks after the reaction. Despite the morphological differences, the new materials maintained their bidimensional structure.

Cyclic voltammograms of the V_2O_5/PEO hybrid compounds are shown in Fig. 6, that of the pure vanadium pentoxide xerogel film ($V_2O_5 \cdot 2.0H_2O$) is depicted in Fig. 7a. The cyclic voltammograms of $V_2O_5 \cdot 2H_2O$ and of the V_2O_5/PEO materials display peaks in the potential range −0.60 V to +1.00 V (SCE), in acetonitrile solution containing 0.1 mol/dm^3 $LiClO_4$. The cyclic voltammogram of the V_2O_5 xerogel film (Fig. 7a) has two cathodic and two

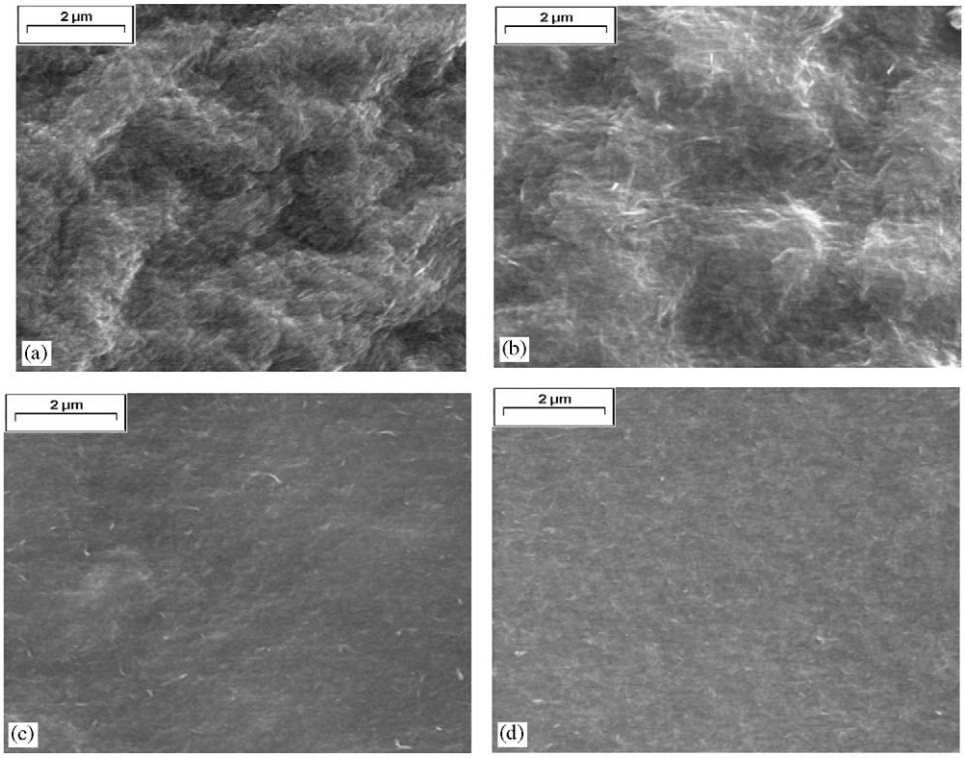

Fig. 5. Scanning electron micrographs of (a) vanadium pentoxide xerogel ($V_2O_5 \cdot 2.0H_2O$); (b) PEOV1160; (c) PEOV3160; (d) PEOV6160.

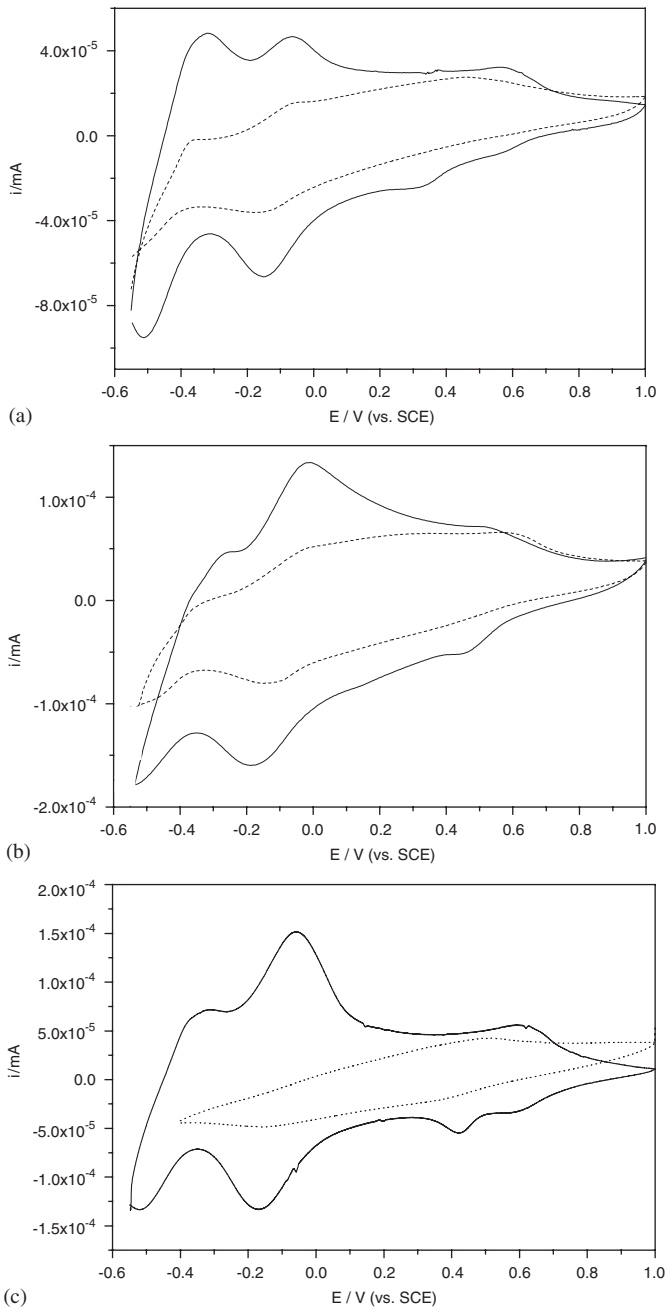

Fig. 6. Cyclic voltammograms of the (a) PEOV125 (solid line) and PEOV1360 (- - -); (b) PEOV325 (solid line) and PEOV3360 (- - -); (c) PEOV625 (solid line) and PEOV6360 (- - -), in acetonitrile, 0.1 mol/dm^3 $LiClO_4$, in the potential range −0.55 to +1.00 V (SCE) and $v = 20$ mV/s.

anodic peaks, ascribed to the $V^V/^{IV}$ redox pair with concomitant occurrence of lithium ion insertion and extraction ($xe^- + xLi^+ + V_2O_5 \cdot nH_2O \rightleftharpoons LixV_2O_5 \cdot nH_2O$). This is a two-step process-taking place in two non-equivalent sites in the vanadium oxide matrix, and the existence of these two sites is probably due to different coordination spheres that maintain the overall electroneutrality of the system [10,40,41]. In addition, the presence of more than one cathodic or anodic current peaks can also be associated with modifications in the structure, which modify the electronic states of the conduction band and allow intercalation/deintercalation of more lithium ions in different sites, compensating for the charge in the film [42]. The cyclic voltammograms of the hybrid compounds (Figs. 6b, d) also show that Li^+ insertion and deinsertion occur in two or three steps during the redox process. The higher potential difference between the cathodic and anodic peak in relation to the vanadium pentoxide xerogel suggests that there is an increase in film resistance, which perhaps results from the difficult lithium diffusion through the film arising from the steric hindrance conferred by the organic polymer. In addition, the width and asymmetric pattern of the waves can be related to the heterogeneity of the film surface. Furthermore, there is a loss of peak definition as well as the current peak intensity in the electrochemical process for the hybrid compounds containing high PEO loading (360×10^{-7} mol/dm^3), as shown in Fig. 6. Thus, composite materials with high content of organic phase lead to lower lithium ion diffusion because of steric interactions, resulting in a poor electrochemical response. However, this effect is less evident for the composite materials with low average molecular weight polymers (Figs. 6a, b). For the xerogel matrix (Fig. 7a), one can verify a decrease in the total charge ($\Delta Q_{total} = 58\%$) after 50 successive voltammetric cycles. This is associated with the loss of peak definition attributed to Li^+ insertion/de-insertion, which is probably due to the production of $Li_xV_2O_5$ stable crystalline phases, thus making the release of lithium ions to the supporting electrolyte solution more difficult [10,26,27]. Besides, Li^+ insertion/deinsertion into the oxide matrix during the redox reaction can promote lattice contraction/expansion. As a result, these volumetric changes after several charge/discharge cycles lead to irreversible structural changes in the V_2O_5 xerogel structure. Concerning the V_2O_5/PEO hybrid compounds (Figs. 7b–d), although the total charge values decrease from the 1st to the 50th cycle, the electrochemical response stabilizes in relation to that of the vanadium pentoxide xerogel. In addition, the total charge variation is lower for the hybrid compounds than for the pure matrix, as can be noted in Table 4. On one hand, this decrease in charge variation can be interpreted as being a result of the presence of the organic polymeric species in the layers, leading to lower Li^+ ion diffusion to the more internal active sites. On the other hand, the presence of the organic phase provides an electrochemically stable process (Table 4) when compared to that obtained with the matrix ($\Delta Q_{total} = 58\%$). It is possible that the presence of the polymer molecules in the V_2O_5 matrix minimize mechanical variations after several charge-discharge cycles, leading to better performance [42]. In other words, the hybrid compound is less susceptible to mechanic stress during Li^+ insertion/deinsertion between the interlayers. In addition, PEO intercalation increases the distance between the V_2O_5 layers, which facilitates the electromigration and accommodation of solvated lithium ions during the intercalation and deintercalation processes, despite the presence of PEO

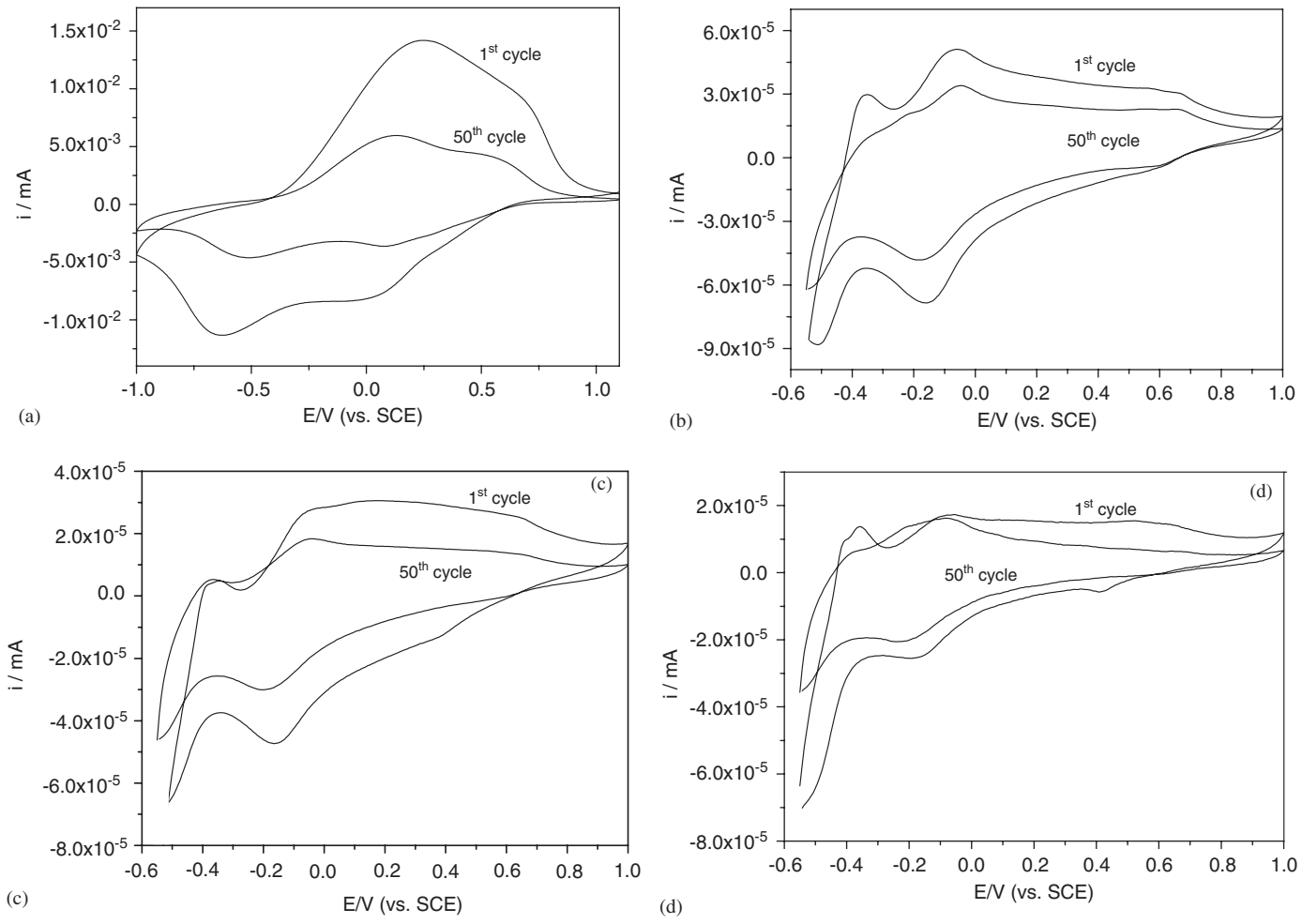

Fig. 7. Cyclic voltammograms and stability essays of the (a) vanadium pentoxide xerogel ($V_2O_5 \cdot 2.0H_2O$; (b) PEOV1160; (c) PEOV3160; (d) PEOV6160 in acetonitrile containing 0.1 mol/dm^3 $LiClO_4$, in the potential range from +1.00 to −0.60 V (SCE) and $v = 20$ mV/s.

Table 4
Values of the total charge variation from the 1st to the 50th cycle of the V_2O_5/PEO hybrid materials with different molecular weights of PEO

Sample	ΔQ_{total} (%)	Sample	ΔQ_{total} (%)	Sample	ΔQ_{total} (%)
PEOV125	52	PEOV325	35	PEOV625	27
PEOV1160	17	PEOV3160	19	PEOV6160	12
PEOV1360	23	PEOV3360	17	PEOV6360	15

molecules. Another possibility stated by Chen et al. [21] is that there is a strong interaction between the host and the guest species, which shields the electrostatic interactions between Li^+ ions and V_2O_5 and results in improved cycling stability.

4. Conclusion

The synthesis, structural and electrochemical properties of vanadium pentoxide xerogel–PEO hybrid materials have been described. In this paper, X-ray diffraction data showed that PEO intercalation retains the lamellar character of the vanadium pentoxide xerogel, although broadening of the X-ray line suggests there is an increase in the layer stacking disorder. The cyclic voltammetry technique demonstrated that PEO intercalation provides an improvement in the electrochemical properties, mainly with respect to the lithium electroinsertion process into the oxide matrix, which occurs with little decrease in total charge during successive redox cycles. However, in the presence of a high content of PEO, a low cyclability is observed due to the higher difficulty of the Li^+ in reaching the more internal active sites.

Acknowledgments

The authors thank Conselho Nacional de Desenvolvimento Científico e Tecnológico (process no. 472848/2004-6) and Fundação de Amparo à Pesquisa do Estado de São Paulo for financial support. Coordenação de Aperfeiçoamento de Pessoal de Nível Superior is gratefully acknowledged for fellowship (EMG). We wish to thank Prof. Dr. C.F.O. Graeff for EPR spectra.

References

[1] H.R. Allock, Science 255 (1992) 1106.
[2] P. Judeinstein, Z. Sanchez, J. Mater. Chem. 6 (1996) 511–525.
[3] P. Gomez-Romero, Adv. Mater. 13 (2001) 163–174.
[4] C. Sanchez, B. Julián, P. Belleville, M. Popall, J. Mater. Chem. 15 (2005) 3559–3592.
[5] V. Manríquez, P. Barahona, D. Ruiz, R.E. ávila, Mater. Res. Bull. 40 (2005) 475–483.
[6] M. Lira-Cantu, P. Gomez-Romero, J. Electrochem. Soc. 144 (1999) 2029–2033.
[7] F. Huguenin, M. Ferreira, V. Zucolotto, F.C. Nart, R.M. Torresi, O.N. Oliveira Chem. Mater. 16 (2004) 2293–2299.
[8] O.Yu. Posudievsky, S.A. Biskulova, V.D. Pokhodenko, J. Mater. Chem. 14 (2004) 1419–1423.
[9] N.G. Park, K.S. Ryu, Y.J. Park, M.G. Kang, D.K. Kim, S.G. Kang, K.M. Kim, S.H. Chang, J. Power Sources 103 (2002) 273–279.
[10] M.A. Gimenes, L.P.R. Profeti, T.A.F. Lassali, C.F.O. Graeff, H.P. Oliveira, Langmuir 17 (2001) 1975–1982.
[11] J. Scarminio, A. Taledo, A.A. Andersson, S. Passerini, F. Decker, Electrochim. Acta 38 (1993) 1637–1642.
[12] P. Soudan, J.P. Pereira-Ramos, J. Farcy, G. Grégoire, N. Baffier, Solid State Ion. 135 (2000) 291–295.
[13] P. Aranda, E. Ruiz-Hitzky, Chem. Mater. 4 (1992) 1395–1403.
[14] P. Aranda, M. Darder, R. Fernández-Saavedra, M. López-Blanco, E. Ruiz-Hitzky, Thin Solid Films 495 (2006) 104–112.
[15] M.X. Reinholdt, R.J. Kirkpatrick, T.J. Pinnavaia, J. Phys. Chem. B 109 (2005) 16296–16303.
[16] L.Q. Mai, W. Chen, Q. Xu, Q.Y. Zhu, Microelectron. Eng. 66 (2003) 199–205.
[17] Y.J. Liu, D.C. DeGroot, J.L. Schindler, C.R. Kannewurf, M.G. Kanatzidis, Chem. Mater. 3 (1991) 992–994.
[18] Y.J. Liu, J.L. Schindler, D.C. DeGroot, C.R. Kannewurf, W. Hirpo, M.G. Kanatzidis, Chem. Mater. 8 (1996) 525–534.
[19] G.M. Kloster, J.A. Thomas, P.W. Brazis, C.R. Kannewurf, D.F. Shriver, Chem. Mater. 8 (1996) 2418–2420.
[20] E. Ruiz-Hitzky, P. Aranda, B. Casal, J. Mater. Chem. 2 (1992) 581–582.
[21] W. Chen, Q. Xu, Y.S. Hu, L.Q. Mai, Q.Y. Zhu, J. Mater. Chem. 12 (2002) 1926–1929.
[22] N. Gharbi, C. Sanchez, J. Livage, J. Lemerle, L. Nejem, J. Lefebvre, Inorg. Chem. 21 (1982) 2758–2765.
[23] J. Livage, Chem. Mater. 3 (1991) 578–593.
[24] C.M. Wu, T.W. Xu, W.H. Yang, J. Solid State Chem. 177 (2004) 1660–1666.
[25] B.B. Owens, S. Passerini, W.H. Smyrl, Electrochim. Acta 45 (1999) 215–224.
[26] K. West, B. Zachau-Christiansen, T. Jacobsen, S. Skaarup, Electrochim. Acta 38 (1993) 1215–1220.
[27] M. Giorgetti, S. Passerini, W.H. Smyl, M. Barrettonni, Inorg. Chem. 39 (2000) 1514–1517.
[28] V. Petkov, P.N. Trikalitis, E.S. Bozin, S.J. Bollinge, T. Vogt, M.G. Kanatzidis, J. Am. Chem. Soc. 124 (2002) 10157–10162.
[29] C. Sanchez, J. Livage, G. Lucazeau, J. Raman Spect. 12 (1982) 68–72.
[30] L. Abello, G. Lucazeau, J. Chim. Phys. 81 (1984) 539–547.
[31] L. Abello, E. Husson, Y. Repelin, G. Lucazeau, J. Solid State Chem. 56 (1985) 379–389.
[32] N. Arun, S. Vasudevan, J. Chem. Phys. 119 (2003) 2840–2848.
[33] W.H.T. Davison, J. Chem. Soc. (1955) 3270–3277.
[34] B.L. Papke, M.A. Ratner, D.F. Shriver, J. Phys. Chem. Solids 42 (1981) 493–500.
[35] J. Selbin, Chem. Rev. 65 (1965) 153–175.
[36] M. Morey, A. Davidson, H. Eckert, G. Stucky, Chem. Mater. 8 (1996) 486–492.
[37] G. Busca, G. Centi, L. Marchetti, F. Trifiro, Langmuir 2 (1986) 568–577.
[38] C. Sanchez, F. Babonneau, R. Morineau, J. Livage, Philos. Mag. B 47 (1983) 279–290.
[39] F. Babonneau, P. Barboux, F.A. Josien, J. Livage, J. Chim. Phys. 82 (1985) 761–766.
[40] M. Nabavi, S. Doeuff, C. Sanchez, J. Livage, Mater. Sci. Eng.-B Solid 3 (1989) 203–207.
[41] R. Baddour, J.P. Pereira-Ramos, R. Messina, J. Perichon, J. Electroanal. Chem. 314 (1991) 81–101.
[42] F. Huguenin, M.J. Giz, E.A. Ticianelli, R.M. Torresi, J. Power Sources 103 (2001) 113–119.